

Synthesis of Lead Titanate Nanostructure by Mechanical Activation Method and Evaluating of its Photocatalytic Decolorization of Methyl orange

E. Khosravipناه^{*1}, S. A. Manafi¹

¹Department of Materials Engineering, Shahrood Branch, Islamic Azad University, Shahrood, Iran.

Received: 10 January 2020 - Accepted: 22 March 2020

Abstract

In this study, lead titanate nanopowder was synthesized using mechanical activation. Raw materials including titanium oxide powder (anatase) and Lead oxide (II) with a ball to powder weight ratio of 1: 10 and the powder ratio of 1:1 were milled in a planetary ball mill for 30 hours. Then, they were heated at 800, 900 and 1000 °C. The volatility of lead and the formation of secondary phases were prevented using this method. The obtained nanopowder was investigated by field emission scanning electron microscope (FESEM), X-ray diffraction (XRD), and Fourier transform infrared spectroscopy (FTIR). The UV absorption spectroscopy was used to calculate the energy gap. Photocatalytic activity of nanopowder by dye degradation of methyl orange under UV light was evaluated. The effects of various influential parameters including initial dye concentration, photocatalyst dose and pH on the dye decolorization were also investigated. The optimum value for initial dye concentration and photocatalyst dose, obtained 10 ppm and 0.042 g, respectively. Also, the best rate of decolorization observed at pH=4. The results suggested that photocatalytic process is a beneficial method for decolorizing methyl orange dye.

Keywords: Lead Titanate Nanopowder, Mechanical Activation, Photocatalyst, Methyl orange.

1. Introduction

The environmental pollution is currently one of the most serious issues faced by the human being. Followed by an ever increasing trend during the recent years, it has reached an alerting level in terms of its impact on the living creatures [1]. Dye-contaminated wastewater from textile industries, which contains chemical contaminants, is one of major environmental pollution with adverse impacts on the humans and the environment.

The dyes not only leak to surface and underground waters to make the water resources dye-contaminated, but also are known to contribute to the incidence of cancers and genetic mutations. Every year, tens of thousands of different types of synthetic dyes are produced around the world, and these productions are widely used in different applications virtually at industries. The textile manufacturing and dyeing industry is a major source of environmental pollution through industrial wastewaters, making them an index of development for any country.

In addition to the textile manufacturing and dyeing industry, some other industries are also producing dye-contaminated wastewater, including the cosmetics, leather, pharmaceuticals, paper, and dye manufacturing industries [2-5].

For instance, about half of the textile dye products are composed of azo compounds with $-N=N-$ chromophore groups on their molecular structure. Some 15% of the total dye produced during the dyeing stage in the textile industry is wasted and disposed in the form of wastewater [6-8]. Various methodologies have been proposed for dye removal from industrial wastewaters, including physiochemical methods such as ultrafiltration [8,9], reverse osmosis [10,11], ion exchange [12], and adsorption on different adsorbents such as active carbon [13], coal [14], wood cuttings [15], and silica gel [16], being relatively successful when it comes to practical use. However, these methodologies are designed to bring the pollution from the aqueous phase to a solid lattice rather than degrading it, keeping them from being comprehensive methods for counterfeiting the pollution [14-16].

Recently, extensive researches are performed to remove pollutants from photocatalytic material. The obtained results indicated that the photocatalytic degradation is an environment-friendly or say green method with no secondary environmental pollution [17,18]. Among the existing methods for removing the environmental pollutions, the use of photocatalytic methods is of paramount importance. The photocatalysts are semiconductors that can oxidize organic compounds when exposed to high-intensity light. When the energy content of a photon exceeds the energy gap (E_g) of the semiconductor, the electron is evoked from the valence band to the conduction band, leaving a cavity in the valence band.

^{*}Corresponding author

Email address: e.khosravipناه@gmail.com

The combination of stimulated electrons and the cavities may lead, either directly or indirectly, to the production of hydroxyl radicals that can, in turn, convert organic matter to mineral matter. An important factor affecting the adsorption process is the choice of adsorbent. Today, ceramic oxides are increasingly used as photocatalytic material. Low cost, availability and outstanding characteristics of these compounds represent their advantageous features [19,20].

With its perovskite structure, the lead titanate nanoceramic (PbTiO₃) is a ferroelectric material that can be used in a wide range of temperatures because of its relatively high curie point of 490°C, as compared to other ferroelectric materials such as SrTiO₃ or BaTiO₃. The lead titanate has outstanding characteristics such as excellent piezoelectric coefficient and large spontaneous polarization [21]. Accordingly, it has numerous potential applications in electronic and microelectronic devices, being a member of the most important families of piezoelectric and ferroelectric materials [22].

Lead titanate exhibits a cubic phase at temperatures beyond 763°C, below which it shows a tetragonal phase. In the tetragonal phase, it shows ferroelectric properties, while it behaves as a para-electric material in the cubic phase. In most cases, the lead titanate undergoes a phase change from para-cubic to tetra-ferroelectric through an anisotropic thermal expansion [23,24].

Nanoparticles of lead titanate can be achieved through different methodologies such as solid-to-solid or liquid-to-solid conversion. Nanoparticle studies have been largely regarded recently. It is a complex task to develop a methodology for producing nanoparticles with accurate adjusted stoichiometry and desirable characteristics.

The choice of mechanical activation as the synthesis method is based on its superiority over other synthesis techniques, rather than economic convenience, this methodology prevents the lead volatility. In the mechanical activation method, the phase formation is accomplished by applying mechanical rather than thermal driving force, while the formation of pure lead titanate nanoceramic requires low-temperature methodologies to control the lead reduction and inhibit the formation of secondary phases. Furthermore, the low reaction temperature for lead titanate manufacturing improves the crystal quality by reducing the deposition pressure. More recently, some researches have been performed on the reinforcing effects of TiO₂ on photocatalytic properties of materials.

In these research projects, the effect of particle size reduction [25], specific surface area increment [26], coupling of the titanium dioxide [27], have been investigated.

The presence of titanium dioxide nano particles in the structure of the lead titanate can provide the lead

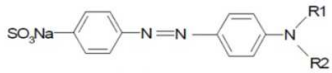
titanate as a nano-photocatalyst because this material has not only desirable electrical and optical properties but also favorable photocatalytic activity. In the present work, the nano-lead titanate is synthesized through mechanical activation and its photocatalytic properties are investigated for degradation of methyl orange dye.

2. Materials and Methods

For synthesis of nano-ceramic lead titanate the raw materials including lead oxide powders (Merck, 99% purity) and anatase-titanium dioxide were put into two separate cups of a ball-milling machine (PF2 model, Farapajhohesh Co., Iran) with ball-to-powder ratio = 10:1. Speed was adjusted on 250 rpm; to prevent of chamber temperature rising, allowed the device to rest for 10 min. for every 30 min. The obtained mixture was milled for 30 h in the ball-milling machine. The prepared specimens were heat treated at 800, 900 and 1000°C in an electric furnace (203 P- LEF, Korea) under ambient atmosphere and nano-ceramic lead titanate was synthesized.

Methyl orange dye was used to study the photocatalytic properties of the specimens ; Table. 1. given methyl orange characteristics.

Table. 1. Methyl orange characteristics[18].

Methyl orange	Molecule
327.33	Molecular weight (g/mol)
465	Maximum wavelength (nm)
	Structure
C ₁₄ H ₁₄ N ₃ NaO ₃ S	Formula

X-ray diffraction analysis was used to investigate the formation of lead titanate phases. The diffraction patterns were recorded in the 2θ range between 10 and 90°. Since in the present study, lead titanate nanoparticles were synthesized by mechanical activation method, Scherrer equation cannot be used to calculate the crystallite size because the prepared specimens contains a lot of stress and strain as a result of milling process and Scherrer equation does not include any (micro) strain effect, so it will not be seen a significant change in the X-ray diffraction patterns of these specimens. Therefore, in order to calculate the crystallite size of specimens, a method should be used to take into account the effect of lattice stress and strain in calculating the crystallite size.

Therefore, the Williamson - Hall method used to calculate the crystallite size of nano-powders. Williamson - Hall equation is Eq. (1). [28] :

$$\beta \cos \theta = \frac{0.9\lambda}{D} + 2\varepsilon \sin \theta \quad \text{Eq. (1)}$$

Where λ is X-ray wavelength (copper lamp with $\lambda = 1.5406\text{\AA}$), D is grain size, ε is strain, β is the width peak at half height and θ is Bragg angle. FESEM (LEO-VP435) and FTIR (JASCO, Japan, 400-4000 cm^{-1}) techniques were used to investigate lead titanate nano-powder morphology and crosslinking bonds as well as present functional groups, respectively. The UV absorption of the specimens were recorded using a UV spectrophotometer (JASCO, V-670) in the wavelength range between 190 and 900 nm. Photocatalytic properties of the specimens were characterized by a UV-Vis spectrometer (Optizen 3320 UV).

3. Results and Discussion

3.1. Identification of Lead Nano-Titanates

Gibbs energy relation was calculated as follows Eq. (2) [29] :

$$\Delta G = \Delta H - T\Delta \quad \text{Eq. (2)}$$

In order to evaluate the reaction feasibility at room temperatures and higher ones, the enthalpy and entropy values at room temperature were placed in the Gibbs energy relation and the free energy was determined. The related negative and positive values ($\Delta S > 0$ and $\Delta H < 0$) show the feasibility of the lead titanate synthesis reaction at the mentioned temperatures. The obtained Gibbs energy was negative which indicates that the reaction is feasible, so synthesis reaction of the lead titanate is a self-activated reaction and if efficient activation energy is applied the lead titanate reactions are feasible. Lead titanate synthesis reaction is as follow Eq.(3):



Reaction of the lead titanate formation is exothermic, so because of it and according to the stoichiometry of lead titanate, production of this nano-powder was performed by the mechanical method. Raw materials, Pbo and TiO_2 , were mixed with a specific molar ratio. The milling time was 30 h to improve the reactivity of the existing material. A complete solid-state reaction can easily occur when the milled particle size can be as large the atomic diffusion mechanism can make an appropriate level of homogeneous mixing. Therefore, it is believed that the solid-state reaction of lead nano-titanate perovskite formation occurs at lower temperatures by decreasing the particle size of oxidized powders. At low temperatures, incomplete lead phase (PbTi_3O_7) arises which has already been reported by some researchers [29,30].

This pyro-chloride phase has a monoclinic structure (a structure with three unequal axes). These observations are mainly attributed not only to the weak reactivity of lead and titanium [31,32] specimens but also the limited capacity of mechanical mixing method [33]. Decomposition of lead oxide is not affected by mechanical energy. Fig. 1. shows the X-ray diffraction pattern of heat treated lead titanate powder at 800 °C, 900 °C and 1000°C. It is obvious that, 800°C has not been a sufficient temperature for synthesis of lead nano-titanate and there are still titanium oxide (anatase) and lead oxide phases in the specimen (Fig. 1-a). By increasing temperature, lead titanate peaks appear at 900°C that indicates the lead nano-titanate formation (Fig. 1-b). With further increase in temperature to 1000°C (Fig. 1-c), the peak intensity has reduced slightly and some of them have removed and the specimen has gone amorphous. By calculating the crystallite size it also observes that an increase of 100°C in heat treatment has increased the crystallite size.

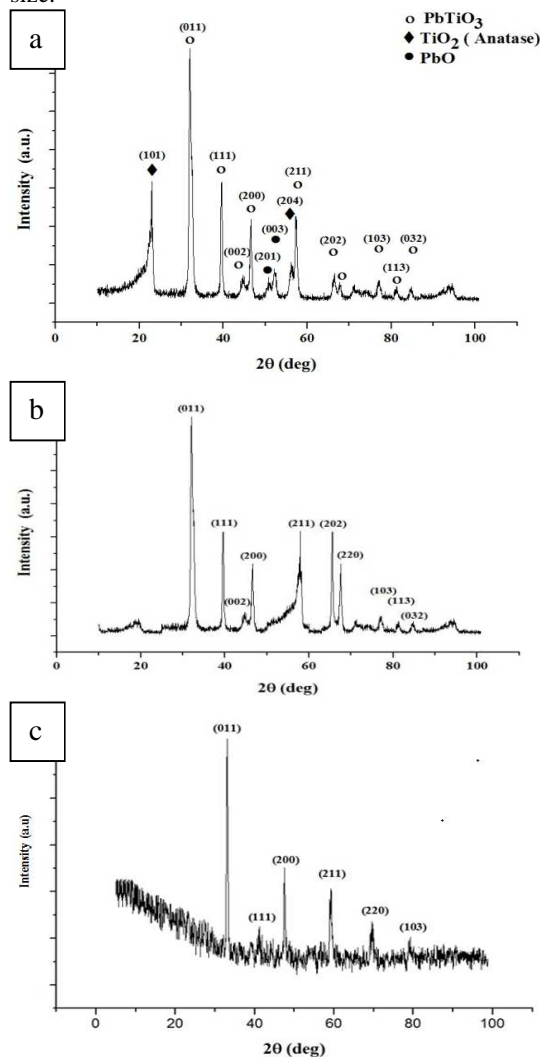


Fig. 1. X-ray diffraction pattern of heat treated lead titanate powder at 800 °C, 900 °C and 1000°C.

Fig. 2. shows Williamson - Hall diagram of the heat-treated lead titanate specimens at 900 and 1000°C. According to this diagram, lattice strain of 0.0127 and the crystallite size of 73 nm (Fig. 2-a). and lattice strain of 0.0141 and the crystallite size of 231 nm (Fig. 2-b). were obtained for 900 °C and 1000 °C, respectively. According to Williamson - Hall diagram, [28] it can be concluded that increasing the temperature increases the crystallite size and also kinetic energy. The particles also start to vibrate which causes crystallites collide to each other, because of stress and strain on the lattice. Therefore, the optimum temperature for the heat treatment of lead titanate powder that has been milled for 30 h was 900 °C. The specimen synthesized at this temperature contains only lead titanate peaks and no secondary phases are formed. Also the size of its crystallites was found in nano limit.

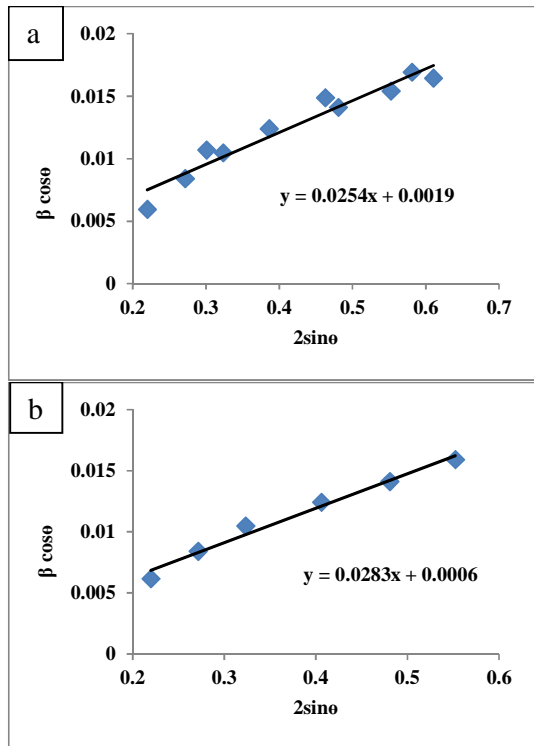


Fig. 2. Williamson - Hall diagram of the heat-treated lead titanate specimens at 900°C and 1000°C.

3.2. Fourier Transform Infrared Spectroscopy

Fig. 3. shows the FTIR curve of TiO_2 and PbO powders mixture. As can be seen, after 30 h of milling and without any heat treatment, the peaks appeared at 1117 cm^{-1} , 1339 cm^{-1} , 1387 cm^{-1} , 1419 cm^{-1} and 1466 cm^{-1} are related to Ti-O bonds and the peaks appeared at 1165 cm^{-1} , 1553 cm^{-1} and 1637 cm^{-1} are related to Pb-O bonds. The peaks also appeared at 562 cm^{-1} and 749 cm^{-1} are related to the metal-oxygen bonds in lead titanate (Fig. 3-a).

Also, it is obvious that, some lead titanate has also been synthesized besides titanium oxide and lead oxide powders. After 30 h of milling and heat treatment at 800°C, the peak of Ti-O is appeared at 1383 cm^{-1} and the peak of Pb-O bonds is appeared at 1633 cm^{-1} , the peaks of 523 cm^{-1} , 637 cm^{-1} and 757 cm^{-1} are related to metal-oxygen bonds in lead titanate (Fig. 3-b). After 30 h of milling and heat treatment at 900°C the peaks of 420 cm^{-1} , 515 cm^{-1} , 646 cm^{-1} and 757 cm^{-1} are related to the metal-oxygen bonds in lead titanate. According to the (Fig. 3-b)., titanium oxide and lead oxide is still present in the combination and the lead titanate phase is not fully synthesized. In contrast, in the (Fig. 3-c). there is no trace of titanium oxide and lead oxide in the combination and the lead titanate phase is almost completely synthesized.

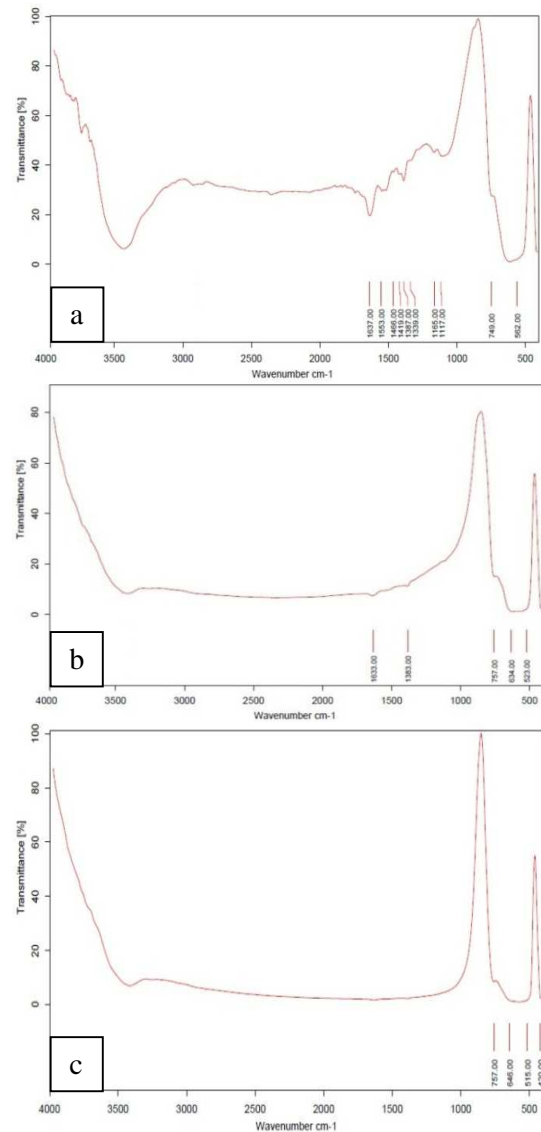


Fig. 3. FTIR curve of TiO_2 and PbO powders mixture after 30 h of milling, a) without any heat treatment, b) 800°C, c) 900°C

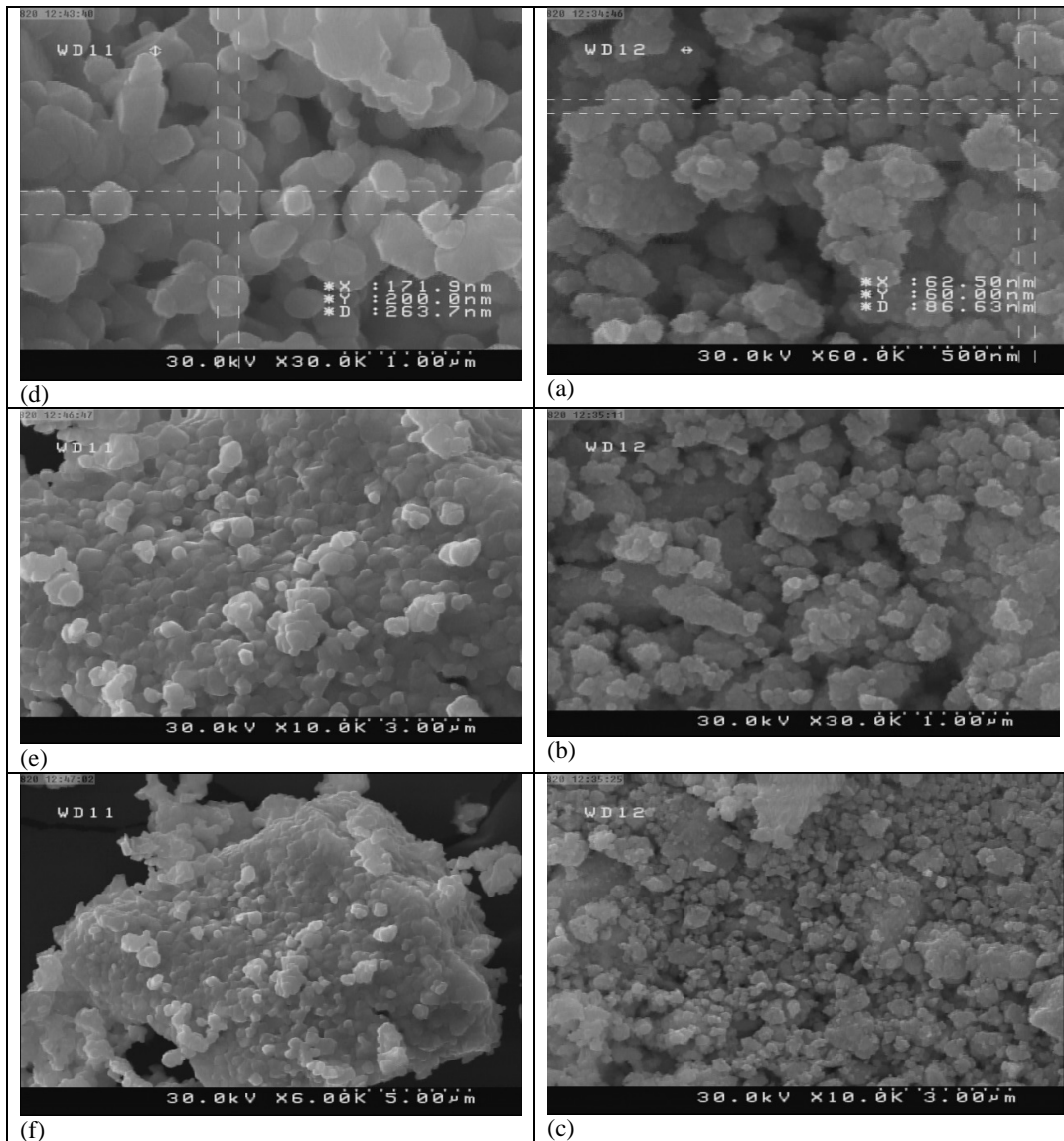


Fig. 4. FESEM images of the lead titanate specimens heat treated at 900 °C., a) 500 nm, b) 1 μ m, c) 3 μ m. And at 1000°C., a) 1 μ m, b) 3 μ m, c) 5 μ m.

3.3. Microstructure

Fig. 4. shows the FESEM images of the lead titanate specimen heat treated at 900°C and 1000°C. FESEM images for both specimens are shown with different magnifications. (Fig. 4-a., Fig. 4-b., Fig. 4-c.) the morphology of some particles are almost spherical as well as some other particles are edged that are expected to be hexagonal lead titanates. It is visible in the images that particles are agglomerated which is expected to be due to the fine particles. Because when the particles size decreases, the surface area of particles increase and with increasing surface energy, the particles tend to reduce their surface energy by accumulation and coalesce and consequently particle agglomeration occurs. In fact,

these agglomerates are very fine particles that are cold welded together.

The agglomerates formed in this specimen are soft agglomerates, so they can be easily separated. Increasing the heat treatment temperature causes an increase in the crystallite sizes and adsorption of small particles and formation of larger particles with clump morphology. Bonding is discussed in agglomerates, so that as the temperature increases, the bonds become stronger and are converted to the covalent and hydrogen bonds. These clump agglomerations are hard agglomerates. Increasing the temperature also has increased the grain with edged morphology and it is expected that the lead titanate phase with hexagonal structure will increase (Fig. 4-d, Fig. 4-e., Fig.4-f.). Therefore, according to the available FESEM images, it can be concluded

that the appropriate temperature for lead titanate nano-powder synthesis is 900°C because an increase of 100°C in temperature causes the structure to be almost out of nano-sized. In some nano definitions, nanoparticles are particles that are smaller than 100 nm. Therefore, this matter also affects the photocatalytic properties of lead titanate powder because increasing the particle size and decreasing the spherical morphology of particles reduces the specific surface area and consequently decreases the photocatalytic properties of the particles.

3.4. Energy Gap Calculation of Lead Nano-Titanate

The energy difference (in units of electron volts) between the highest valence bond and the lowest conduction bond is called bond gap energy. The reflective influence of spectroscopy is used to determine the energy bond gap and it can be calculated from Eq. 4. [34]:

$$ah\nu = C(h\nu - E_g)^{1/2} \quad \text{Eq. (4)}$$

where α is the linear absorption coefficient, h is the Planck constant, ν is frequency (generally $h\nu$ denotes the energy of the photon function), C is the proportional constant and E_g is the energy bond gap. According to Fig. 5. the wavelength of the absorption edge was obtained 390 nm [35] for lead titanate using Eq. 4.; by placing this wavelength of absorption edge in the Eq. 5. the energy gap is estimated 3.17 eV. This indicates the applicability of lead titanate in the photocatalytic field[34]:

$$E(eV) = \frac{1240}{\lambda(nm)} \quad \text{Eq. (5)}$$

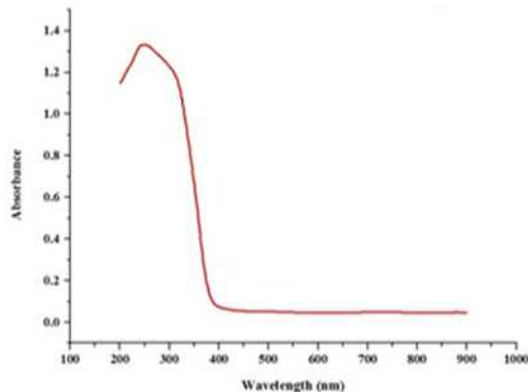


Fig. 5. Absorption spectroscopy of lead titanate.

3.5. Photocatalytic Properties

Methyl orange dye concentration of the specimens was measured using UV-Visible spectrometer and the standard curve drawn at 465 nm wavelength. Eq. 6. was used to determine residual methyl orange

concentration in the absorption and decomposition processes[35]:

$$A = 0.075 C \quad \text{Eq. (6)}$$

Where A is absorption and C is dye concentration. In order to obtain the optimum amount of photocatalyst, 0.014 g, 0.028 g, 0.042 g and 0.056 g of lead titanate photocatalyst was added to 10 ml solution of 10 mg/l of methyl orange and the specimens were stirred magnetically under UV light for 30 min, 60 min, 90 min, 120 min and 150 min, respectively. Subsequently, the photocatalyst was separated by centrifuge and dye absorption at 465 nm wavelength was recorded by UV-Visible. The percentage of methyl orange dye degradation was calculated by the Eq. 7. [36]:

$$D(\%) = \frac{C_0 - C_t}{C_0} \times 100 \quad \text{Eq. (7)}$$

Where C_0 is initial concentration, C_t is concentration at instant t and D is percentage of methyl orange dye degradation.

Fig. 6. shows the percentage of methyl orange dye degradation versus the photocatalyst amount. As can be seen in Fig. 6., by increasing the amount of photocatalyst the rate of removal increases. This increase is due to an increment in active surface (available sites) and increase in hydroxyl radicals (OH^\bullet) and the super oxide radicals (O_2^\bullet), respectively. This ascending rate continues until reaches to a maximum of photocatalyst at 0.042 g and then the absorption decreases by further increasing amount of nanophotocatalyst. This phenomenon can be attributed to the interaction between available sites and the turbidity caused by increment of photocatalyst. It can be concluded that, the reason for reducing the degradation is large amounts of photocatalyst (more than 0.042 g) that acts as a filter and prevent light to reach the other solution sides [36]. regarding to the obtained these results optimal photocatalyst amount is 0.042 g.

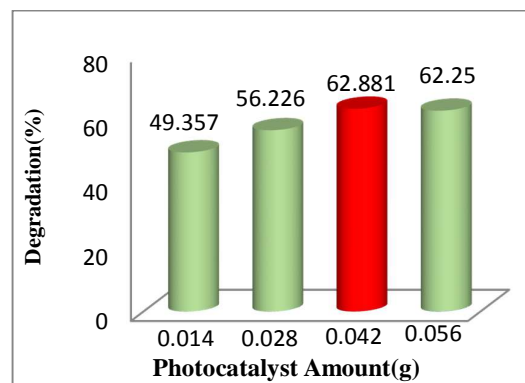


Fig. 6. The effect of lead titanate photocatalyst amount on the methyl orange dye degradation.

In order to evaluate the effect of methyl orange dye concentration on the degradation reaction.

10 ml of 5 mg/l, 10 mg/l, 20 mg/l, 30 mg/l and 40 mg/l of methyl orange solution with the optimal value of 0.042 g photocatalyst was exposed under UV irradiation.

Fig. 7. shows the effect of methyl orange dye concentration on the degradation reaction.

As can be seen in this figure, by increasing the dye molecules concentration under the same conditions photocatalytic system needs more exposure time to decolorate and reach the same percentage of degradation [37].

By increasing the dye concentration, the light photons absorb by the dye molecules before they reach the photocatalyst surface. Lack of sufficient light in photocatalyst surface in a high concentration of dye has a directly effect on the production of $\cdot O_2^-$ and $\cdot OH$ radicals and decreases the ratio of these oxidant radicals concentration and dye molecules.

In addition, production and migration of electron pairs – produced hole are also occurred more slowly which is due to a reduction in the absorbed photons. By increasing the initial dye concentration, probability of interaction between dye molecules and oxidant radicals decreases [38]. Furthermore, intermediate products formed by decomposition of dye molecules are also increased. So there is a competition for decomposition between these intermediate materials produced by mother dye molecules [39]. Subsequently, it is not unexpected that the overall rate of photocatalytic reaction, namely the degradation of methyl orange dye, will decrease.

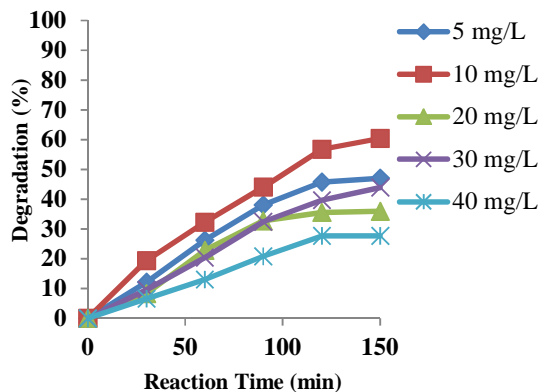


Fig. 7. The effect of methyl orange on the methyl orange dye degradation.

According to the Langmuir - Hinshelwood equation the decomposition process follows a first order kinetic [40]. In addition, linear curve shows that the decomposition process is occurred on the photocatalyst surface. Fig. 8. shows the results of 5 mg/l, 10 mg/l, 20 mg/l, 30 mg/l and 40 mg/l methyl orange concentrations in presence of 0.042 g of lead titanate photocatalyst based on the Langmuir-Hinshelwood equation. Additionally, the results of

this figure show that, the decomposition rate of 10 mg/l concentration of methyl orange is more than 5 mg/l, 30 mg/l, 20 mg/l and 40 mg/l concentrations; their reaction rate constant are obtained 0.005 min^{-1} , 0.004 min^{-1} , 0.004 min^{-1} , 0.003 min^{-1} and 0.002 min^{-1} , respectively.

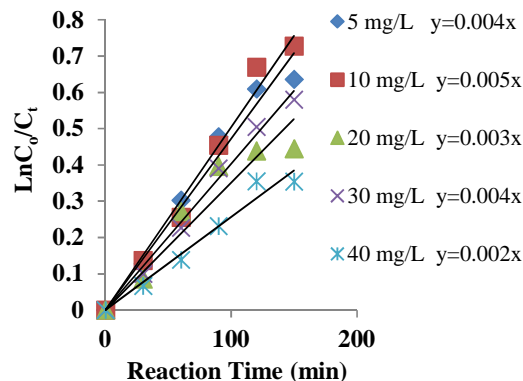


Fig. 8. Methyl orange dye degradation kinetics.

In order to evaluate the effect of pH on the dye degradation performance using lead nano titanate, the dye degradation process have been conducted at 4 and 9 pHs with a 10 mg/l concentration of methyl orange solution and 0.042 g of photocatalyst. It should be noted that pH of methyl orange solution was 6.5. Fig. 9. shows the obtained results, pH of media not affects on the dye structure but it affects on the photocatalyst surface charge. Furthermore, the results shows that the degradation in the acidic media is more than a neutral or basic media; photocatalyst surface will be protonated in the acidic media (OH_2^+ on the photocatalyst surface), so methyl orange that is an anionic dye will be absorbed better on the photocatalyst surface. In the basic media, photocatalyst surface has a negative charge because the hydrogen that attached to the oxygen on the photocatalyst surface detaches by the base and the photocatalyst surface becomes negative. Electrostatic repulsion between anionic dye and photocatalyst surface can inhibit the absorption.

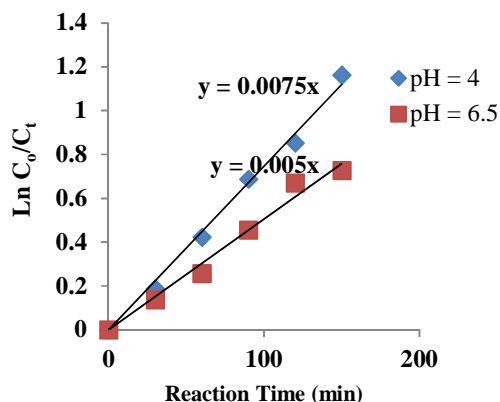


Fig. 9. Methyl orange dye degradation kinetics at 4 and 9 pHs.

Fig. 10. shows the effect of reaction temperature on the percentage of methyl orange dye degradation by lead nano titanat. For this purpose, 0.042 g of photocatalyst is added to a 10 mg/l solution of methyl orange with pH=4 and the specimen was stirred for 150 minutes under UV light.

The experiments were performed at 25 °C, 30 °C, 40 °C and 50 °C. Low temperature dependence of the degradation rate reflects the fact that the degradation is a quite optical reaction, so the temperature dose not a significant effect on the degradation reaction of methyl orange dye and consequently room temperature was selected for the experiments.

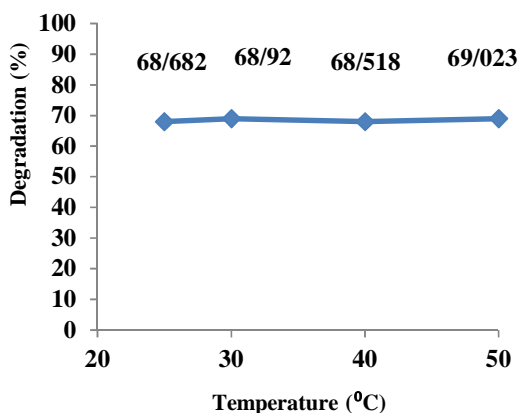


Fig. 10. The effect of reaction temperature on the percentage of methyl orange dye degradation by lead nanotitanate.

4. Conclusions

1. The degradation of methyl orange dye was investigated by lead nanotitanate. For this purpose lead nanotitanate after the heat treatment was synthesized at 900°C; because at this temperature there are no trace of the original compounds of titanium oxide and lead oxide and it seems that the lead titanate is completely synthesized and other secondary phases have not existed.

2. According to Hull Williamson method, the average crystallite size obtained 73 nm. In order to predict of the photocatalytic ability, the energy gap was determined around 3.17 eV according to UV-Visible analysis.

3. The results show that the optimum initial concentration of dye and the photocatalyst are 10 ppm and 0.042 g, respectively and degradation in an acidic media is more than a neutral and basic media. Degradation process follows a first order kinetic.

4. The morphology of some particles were almost spherical and the other ones had edges which related to hexagonal lead titanate particles. In this study, no effects of adding impurities in the calcined powders due to corrosion residual of the milling process were not defected, so it confirms that this technique is useful for production of lead nanotitanate powders.

References

- [1] A. Nagham and A. Ageena, *J. Eng. Technol.*, 28, (2010), 859.
- [2] P. Niu and J. Hao, *Colloids Surf A: Physicochem. Eng. Asp.*, 431, (2013), 127.
- [3] P. Zhang, Q. An, J. Guo and C. C. Wang, *Colloid Interf. Sci.*, 389, (2013), 10.
- [4] D. Zhao, W. Zhang, X. Wang and C. Chen, *Procedia Environ. Sci.*, 18, (2013), 890.
- [5] B. Royer, N. F. Cardoso, E. C. Lima, V. S. O. Ruiz, T. R. Macedo and C. Airoidi, *Colloid Interf. Sci.*, 336, (2009), 398.
- [6] Z. Zhang, Y. Xu, X. Ma, F. Li, D. Liu, Z. Chen, F. Zhang and D. D. Dionysiou, *J. Hazard. Mater.*, 271, (2012), 209.
- [7] H. Zhu, R. Jiang, Y. Fu, Y. Guan, J. Yao, L. Xiao and G. Zeng, *Desalination.*, 286, (2012), 41.
- [8] M. Bielska and J. Szymanowski, *Water Res.*, 40, (2006), 1027.
- [9] Katarzyna Majewska-Nowak, *Desalination*, 221, (2008), 395.
- [10] N. Al-Bastaki, *Chem. Eng. Process.: Process Intensification*, 43, (2004), 1561.
- [11] S. K. Nataraj, K. M. Hosamani and T. M. Aminabhavi, *Desalination*, 249, (2009), 12.
- [12] W. Jeng-Shiou, L. Chia-Hung, Ch. Khim Hoong and S. Shing-Yi, *J. Membrane Sci.*, 309, (2008), 239.
- [13] Ch. Suhong, Zh. Jian, Zh. Chenglu, Y. Qinyan, L. Yan and L. Chao, *Desalination*, 252, (2010), 149.
- [14] L. Zhuannian, ZH. Anning, W. Guirong and ZH. Xiaoguang, *Chin. J. Chem. Eng.*, 17, (2009), 942.
- [15] O. E. Augustine, *Chem. Eng. J.*, 143, (2008), 85.
- [16] L. Jinshui, M. Shi and Z. Lingjie, *Appl. Surf. Sci.*, 265, (2013), 393.
- [17] W. J. Tseng and R. D. Lin, *J. Colloid Interf. Sci.*, 428, (2014), 95.
- [18] W. Hao, Y. Xi, J. Hu, T. Wang, Y. Du and X. L. Wang, *J. Appl. Phys.*, 111, (2012), 07B301.
- [19] G. Corro, U. Pal and N. Tellez, *Int. J. Anal. Chem.*, 4, (2013), 125.
- [20] C. Ren, B. Yang, M. Wu, J. Xu, Z. Fu and T. Guo, *J. Hazard. Mater.*, 182, (2010), 123.
- [21] J. Wang, J. Li and Y. W. Wang, *Mech. Mater.*, 331, (2013).
- [22] J. Kennedy, J. Leveneur and P. P. Murmu, AamirIqbal, *Int. J. Chemtech. Res.*, 7, (2015), 90-593.
- [23] Y. Wang, L. Yang and X. Wang, *J. Ceram. Process. Res.*, 14, (2013), 1.
- [24] K. Valdimir, *Process. Appl. Ceram.*, 6, (2012), 37.
- [25] A. Talebian, M. H. Entezari and N. Ghows, *Chem. Eng. J.*, 229, (2013), 304.
- [26] Sh. Zheng, L. Gao, Q. H. Zhang and J. K. Guo, *J. Mater. Chem.*, 10, (2000), 723.

- [27] M. Viviana, M. Silva. Rocha, P. Godoi, T. Leonardo. Ribeiro, O. Marluce and S. Guarda, *Mater. Sci. Eng.: B*, 185, (2014), 13.
- [28] V. D. Mote, Y. Purushotham, B. N. Dole, *J. Theory. Appl. Phys.*, 6, (2012).
- [29] J. Tartaj, C. Moure, L. Lascano and P. Duran, *J. Mater. Res. Bull.*, 36, (2001), 2301.
- [30] M. L. Calzada, M. Alguero and L. Pardo, *J. Sol-Gel Sci. Technol.*, 13, (1998), 837.
- [31] A. Udomporn and S. Ananta, *Appl. Phys.*, 4, (2004), 186.
- [32] A. Udomporn and S. Ananta, *Mater. Lett.*, 58, (2003), 1154.
- [33] S. Ananta, R. Tipakontitikul and T. Tunkasiri, *Mater. Lett.*, 57, (2003), 2637.
- [34] H. He, J. Yin, Y. Li, Y. Zhang, H. Qiu, J. Xu, T. Xu and C. Wang, *Appl. Catal. B: Environ.*, 156, (2014), 35.
- [35] Y. Huang, Y. Cai, D. Qiao and H. Liu, *Particuology*, 9, (2011), 170.
- [36] M. E. Olyaa, A. Pirkarami, M. Soleimani and M. Bahmaei, *J. Environ. Manage.*, 121, (2013), 210.
- [37] I. K. Konstantinou and T. A. Albanis, *Appl. Catal. B*, 49, (2004), 1.
- [38] B. Krishnakumar, K. Selvam, R. Velmurugan and M. Swaminathan, *Desalin. Water Treat.*, 24, (2010), 132.
- [39] J. M. Lee, M. S. Kim, B. Hwang, W. Bae and B. W. Kim, *Dyes Pigments J.*, 56, (2003), 59.
- [40] D. A. Silva and C. G. Faria, *J. Photoch. Photobio.*, 155, (2003), 133.